

Realistic interference-free channel assignment for dynamic wireless mesh networks using beamforming



Aizaz U. Chaudhry*, Roshdy H.M. Hafez, John W. Chinneck

Department of Systems and Computer Engineering, Carleton University, Ottawa, Canada

ARTICLE INFO

Article history:

Received 2 September 2015

Revised 13 July 2016

Accepted 2 August 2016

Available online 2 August 2016

Keywords:

Beamforming

Channel assignment

Wireless mesh networks

ABSTRACT

To make the most efficient use of scarce bandwidth, channel assignment methods for wireless mesh networks (WMNs) should try to minimize the number of frequency channels used while achieving maximum network throughput. Beamforming is a well-known technique that improves spatial reuse in wireless networks. However, there are no channel assignment methods for WMNs that use beamforming to reduce the number of frequency channels. We develop the first channel assignment method for dynamic WMNs that incorporates beamforming in the conflict graph and matrix. This reduces co-channel interference significantly, thereby reducing the *number of frequency channels required* (NCR) to ensure interference-free communication among the mesh nodes while achieving maximum network throughput. Our novel *Linear Array Beamforming-based Channel Assignment* (LAB-CA) method significantly increases the spectrum utilization efficiency of WMNs at the expense of increased hardware complexity. It outperforms classical *omni-directional antenna pattern-based channel assignment* (OAP-CA) in terms of NCR. In a heterogeneous WMN where mesh nodes have differing numbers of radio interfaces, LAB-CA also outperforms OAP-CA in terms of NCR in both sparse and dense scenarios. A further significant reduction in NCR is achieved when the number of antennas in the linear antenna arrays of mesh nodes is increased.

© 2016 Elsevier B.V. All rights reserved.

1. Introduction

It is well known that co-channel interference in wireless networks degrades network throughput. The goal of an effective channel assignment method for multi-radio multi-channel (MRMC) wireless mesh networks (WMNs) is to minimize the number of frequency channels required for interference-free communication among the mesh nodes while achieving maximum network throughput. Beamforming mitigates interference in wireless networks by improving spatial reuse. The full potential of beamforming in WMNs cannot be realized until methods are developed that accurately capture its characteristics in their interference models to minimize the number of frequency channels. To the best of our knowledge, no existing channel assignment method for MRMC WMNs incorporates the necessary beamforming-based interference modeling.

We develop a new and effective channel assignment method that minimizes the *number of frequency channels required* (NCR) to ensure interference-free communication among the mesh nodes for achieving maximum network throughput in a dynamic MRMC

WMN. Our novel *Linear Array Beamforming-based Channel Assignment* (LAB-CA) method is the first of its kind to incorporate beamforming in the conflict graph and matrix to minimize co-channel interference and to reduce NCR. As expected, the results show that LAB-CA significantly outperforms classical *omni-directional antenna pattern-based channel assignment* (OAP-CA) in terms of NCR. Preliminary work in this regard appears in [1].

The node-degree of a mesh node is the number of radio interfaces that it has for data communication with its neighbors. In a WMN architecture consisting of *homogeneous mesh nodes*, the node-degree of all mesh nodes is the same. We also study a more realistic WMN architecture consisting of *heterogeneous mesh nodes* (i.e. mesh nodes having different node-degrees). We extend LAB-CA to incorporate heterogeneous mesh nodes and evaluate its performance in homogeneous vs. heterogeneous environments. We find that *LAB-CA for heterogeneous mesh nodes* (LAB-CA_{HT}) requires more frequency channels as compared to *LAB-CA for homogeneous mesh nodes* (LAB-CA_{HG}).

We also evaluate the performance of LAB-CA_{HT} by comparing its performance with *OAP-CA for heterogeneous mesh nodes* (OAP-CA_{HT}) in both sparse and dense WMNs. We find that LAB-CA_{HT} outperforms OAP-CA_{HT} in terms of NCR in both scenarios. It performs even better in dense mesh networks and provides a reduction of at least 58% in NCR.

* Corresponding author.

E-mail addresses: auhchaud@sce.carleton.ca (A.U. Chaudhry), hafez@sce.carleton.ca (R.H.M. Hafez), chinneck@sce.carleton.ca (J.W. Chinneck).

In a *multi-radio multi-channel multi-antenna* (MRMCMA) WMN, the number of antennas in the linear antenna array of a multi-radio mesh node is greater than its node-degree. We explore the impact of increasing the number of antennas in the linear antenna arrays of the multi-radio mesh nodes on the number of frequency channels when using LAB-CA_HT in a MRMCMA WMN. We find that a further significant reduction of at least 20% in NCR is achieved when the number of antennas in the linear antenna arrays of mesh nodes exceeds their node-degrees.

Specifically the main contributions of this paper are as follows:

- A new and effective channel assignment method LAB-CA is proposed and evaluated. It incorporates beamforming directly into the conflict graph and matrix for modeling interference in MRMC WMNs as a means to minimize co-channel interference and to reduce the total number of required frequency channels.
- To model a more realistic WMN architecture, the channel assignment framework is extended to incorporate heterogeneous mesh nodes, and the effectiveness of LAB-CA_HT in sparse as well as dense mesh networks is demonstrated.
- A multi-radio multi-channel multi-antenna WMN architecture is proposed, and the effectiveness of using multi-antenna mesh nodes is demonstrated.

The rest of the paper is organized as follows. Section 2 presents the related work in this area. Our model for the network architecture is presented in Section 3. The LAB-CA method is presented in Section 4. The extension of the channel assignment framework that incorporates heterogeneous mesh nodes and consists of LAB-CA_HT is presented in Section 5. Performance evaluation with results is given in Section 6. Conclusions are presented in Section 7.

2. Related work

Channel assignment schemes [2–18] for classical MRMC WMNs typically assume a multi-radio mesh node to be equipped with omni-directional antennas. Using these, a mesh node can communicate with several neighbors simultaneously over different frequency channels. When a pair of mesh nodes are communicating over a certain frequency channel, other mesh nodes within the circular radiation pattern of their omni-directional antennas must not transmit over the same frequency channel to avoid a conflict.

To improve spatial reuse by reducing co-channel interference, DMesh [19] proposes the use of directional antennas for mesh nodes in a MRMC WMN. Directional antennas are used in [20] for directional transmission and reception algorithms for wireless ad-hoc networks. A study of the joint routing and scheduling optimization problem in TDMA-based WMNs [21] assumes that nodes are equipped with directional antennas. In [22], the authors study the problem of building topologies for nomadic WMNs where the degree of any node is less than its number of available directional mesh radios. A topology control method for MRMC WMNs that use directional antennas is proposed in [23]; however such antennas are non-steerable and always point where they were manually directed at the time of installation. Hence they are not useful in a dynamic WMN environment undergoing regular topological changes as new mesh nodes join the network or existing mesh nodes leave it, e.g. due to node failure.

For the successful operation of a self-organizing and dynamic MRMC WMN, beamforming is required instead of directional antennas with stationary radiation patterns. Multiple beams can be formed by using the multiple omni-directional antennas of a multi-radio mesh node in the form of a linear antenna array. Unlike the non-steerable beam of a directional antenna such as a parabolic antenna, the main beam of a linear antenna array can be pointed in any desired direction by controlling the progressive

phase difference between the antenna elements of the array. This steerable beam pattern of a linear antenna array can be used in the operation of a dynamic WMN.

Schemes that use beamforming for interference mitigation have been proposed in the literature for TDMA-based single-radio single-channel multi-hop wireless networks [24,25], cellular networks [26], and single-hop wireless ad-hoc networks [27]. In [24], the spatial-reuse-only protocol is proposed, which uses multiple antennas of a wireless node for beamforming to prevent a transmitter's signal from reaching nearby undesired receivers. A multi-antenna beamforming technique is described in [25] to suppress interference and improve spatial reuse. Both [24] and [25] use the protocol model [28] for interference. The authors study a joint base-station association, beamforming, channel assignment and power control problem in heterogeneous cellular networks in [26], where low-power base-stations are overlaid with conventional macro base-stations. The problem of interference suppression is considered in [27] and a joint iterative beamforming and channel allocation strategy is proposed for wireless nodes in an ad-hoc network, where pairs of nodes communicate only with each other. It is assumed that the available frequency band is divided into orthogonal frequency channels of the same bandwidth, and each node is capable of switching between two orthogonal frequencies. Unlike these schemes [24–27], this work deals with the problem of channel assignment in multi-hop multi-radio multi-channel WMNs, where the objective is to assign frequency channels to those links between multi-radio mesh nodes that are required to achieve maximum network throughput such that all of these links can be active simultaneously without any co-channel interference. To the best of our knowledge, LAB-CA is the first channel assignment method of its kind that incorporates beamforming directly in the conflict graph and matrix to significantly reduce the number of frequency channels required for interference-free channel assignment in dynamic MRMC WMNs.

Similar to LAB-CA_HG, the channel assignment schemes in [3,4,8,10,13,17] assume that the node-degrees of all mesh nodes in the network are the same. The topology-controlled interference-aware channel-assignment algorithm (TICA) [3] uses four radio interfaces at each mesh node. The breadth-first-search channel assignment (BFS-CA) scheme [7] requires that a certain number of mesh routers with a certain number of radio interfaces are placed at certain hops from the gateway, whereas LAB-CA_HT does not require any careful mesh router placement strategy. While evaluating the performance of the max-flow-based channel assignment and routing (MCAR) scheme [9], the authors consider two classes of topologies with 25 and 50 mesh nodes. In the 25-node network, 60% of the mesh routers are assigned 2 radios while the remainder are assigned 3 radios. In the 50-node network, 20% of nodes have 2 radios, 40% have 3 radios and 40% have 4 radios. For each class, 20 different topologies are generated having different placements of nodes. LAB-CA_HT works with any random number of radio interfaces at the mesh nodes; in our experiments we choose this number from a uniform random distribution.

Different channel assignment schemes have used different WMN sizes in their performance evaluations. The centralized hyacinth (C-HYA) scheme [4] used a 100-node mesh network. The distributed hyacinth (D-HYA) scheme [6] used a 60-node mesh network. A topology consisting of 30 mesh nodes was used for the performance evaluation of BFS-CA. The simulation experiments on the traffic and interference aware channel assignment scheme (MesTiC) [8] used a 25-node mesh network. TICA was evaluated using a 36-node mesh network. Two classes of topologies with 25 and 50 mesh nodes respectively were used to evaluate MCAR. In [17], two different deployments consisting of 36 and 60 mesh nodes were used. The channel assignment method is simulated using two sets of networks in [10]; the dense network has 50 mesh

nodes in a 500×500 square meter area and the sparse network has 50 mesh nodes in an 800×800 square meter area. To evaluate the performance of LAB-CA_HT, our experiments use 36 mesh nodes distributed in a 500×500 square meter area for the sparse network and 100 mesh nodes distributed in the same area for the dense network.

3. Network architecture

Each mesh node is assumed to be equipped with multiple radio interfaces. One of these radios is used for control traffic (*control radio*), while the others are used for data traffic (*data radios*). The *node-degree* of a mesh node is defined as the number of neighbors it can communicate with simultaneously for data communication. For example, a node-degree of three means that a mesh node is equipped with three data radios and one control radio, and can communicate with at most three of its neighbors at the same time.

The radio interfaces are assumed to be half-duplex and each is equipped with an omni-directional antenna. They can be tuned to different frequency channels. For communication of the control traffic, the control radios of all nodes are tuned to a common frequency channel.

We assume that the antennas of the data radios of a mesh node can be arranged in the form of a linear antenna array for beamforming. Using multiple beams equal to the number of omni-directional antennas in its array, a mesh node can communicate with multiple neighbors simultaneously over different frequency channels. For example, a mesh node with a node-degree of four has four data radios and four antennas in its array. Using all four antennas, the mesh node can form up to four beams to communicate with up to four neighbors simultaneously over four different frequency channels.

In a homogeneous WMN, the node-degrees of all mesh nodes in the network are the same. In a heterogeneous WMN, mesh nodes have different node-degrees chosen using a uniform random distribution between two and some upper limit. A single mesh gateway (GW) is assumed and all mesh nodes, except the GW, are assumed to be sources of flow (i.e. data traffic). The GW is the sink of all flows and hence the maximum possible network throughput depends on its node-degree. For a fair comparison of LAB-CA_HG and LAB-CA_HT, we assume that the GW has the highest node-degree in the heterogeneous architecture. For example, in a heterogeneous mesh network where the node-degree is randomly chosen between two and four, the node-degree of the GW is four.

In LAB-CA_HG, when the node-degree of all mesh nodes is six and a mesh node needs to communicate with two neighbors simultaneously, it uses all antennas of its six-antenna array to form two beams directed towards the two neighbors. On the other hand, in LAB-CA_HT, when the node-degree of a mesh node is randomly selected between two and six, and a mesh node is assigned a node-degree of three and needs to communicate with two neighbors simultaneously, then it uses all antennas of its three-antenna array to form two beams directed towards its two neighbors. The beam formed by a six-antenna array is more focused than that formed by a three-antenna array. This concept is illustrated in Fig. 2 in Section 5.3.

4. Linear array beamforming-based channel assignment

To find the true minimum number of frequency channels required for interference-free communication among mesh nodes, the channel assignment problem should be formulated as a single integrated problem. However, this makes the problem too complex, especially the minimum coloring part, which is well-known to be NP-hard [29]. For this reason, the problem is broken down into stages. Our channel assignment framework consists of four

stages: connectivity graph construction, routing, interference modeling, and minimum coloring.

4.1. Connectivity graph

To minimize the number of frequency channels required, we use our *Select x for less than x* topology control algorithm (TCA) [2] to build the connectivity graph $C(V,E)$, where vertices V correspond to wireless nodes, and edges E correspond to the wireless links between nodes. This algorithm controls the network topology by selecting the nearest nodes as communication neighbors for each node in the network. Since transmit power is proportional to the distance between the nodes, the shorter the distance, the lower the transmit power. Less transmit power translates to less interference, which leads to better spatial reuse.

4.2. Multi-path routing

To achieve maximum network throughput, we formulate the multi-path routing problem as a mixed integer linear program as in [11]. Given the connectivity graph, the objective is to maximize the network throughput while maintaining fairness among the multiple network flows. *Network throughput* means the total amount of flow that reaches the single gateway from all sources. We must also satisfy flow conservation, node-degree, half-duplex, fairness, and link capacity constraints on the connectivity graph.

We assume a link capacity based on the fact that maximum goodputs (maximum link throughputs) of an IEEE 802.11a link operating at data rates of 12, 24, 36, and 54 Mbps are 9.18, 15.52, 20.03, and 24.73 Mbps, respectively [18,30]. We use the AMPL language [31] to model the multi-path routing problem, and IBM CPLEX 12.2 [32] to solve the resulting problem.

4.3. Interference modeling

4.3.1. Linear antenna array design

Each mesh node is equipped with multiple radio interfaces and each radio interface is equipped with an omni-directional antenna. Note that a vertically polarized half-wavelength dipole antenna is an omni-directional antenna in the ϕ -plane, i.e. at elevation angle $\theta = 90^\circ$.

The multiple antennas of a mesh node constitute a linear antenna array. The array consists of N_a elements equally spaced at a distance d_a apart. The antenna elements are positioned along the x -axis. The distance d_a between the elements in the array is $\lambda/2$. All elements have identical amplitudes of the excitation current. The phase by which the current in each element leads the current of the preceding element is the same. The elements in the array are half-wavelength dipoles. The first element of the array is located at the origin. Far-field conditions are assumed. The antenna elements are assumed to be lossless. There is no mutual coupling between antenna elements of the array. The height of the linear antenna array of a mesh node from the ground is the same for all nodes, and a mesh node needs to steer its beams in the ϕ -plane only to communicate with its neighbors, hence it is required to find the array gain only in the ϕ -plane. The antenna elements are vertically polarized, which means that the antenna elements of the array of a mesh node are oriented parallel to the z -axis. The array gain AG of this linear antenna array in the ϕ -plane can be written as [1]

$$AG(\theta = \pi/2, \phi) = \frac{1}{N_a} G_o |AF(\theta = \pi/2, \phi)|^2, \quad (1)$$

where G_o is the maximum gain of a half-wavelength dipole, and AF is the array factor in the ϕ -plane and is given by [33]

$$AF(\theta = \pi/2, \phi) = 1 + e^{jk d_a (\cos \phi - \cos \phi_0)} + e^{j2k d_a (\cos \phi - \cos \phi_0)} + \dots + e^{j(N_a - 1)k d_a (\cos \phi - \cos \phi_0)} \quad (2)$$

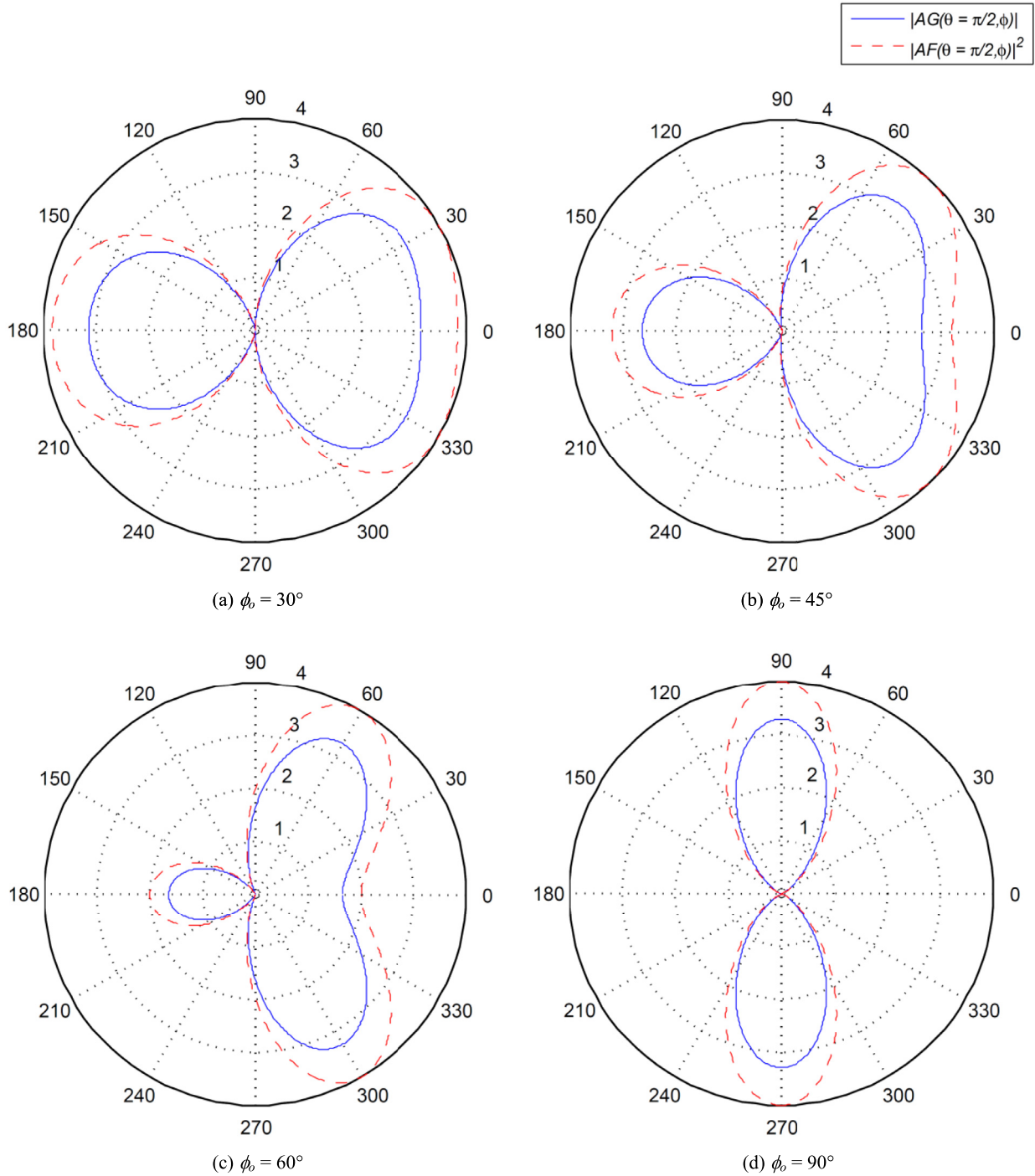


Fig. 1. Plot of $|AF(\theta = \pi/2, \phi)|^2$ and $|AG(\theta = \pi/2, \phi)|$ for different values of ϕ_0 ($N_a = 2$).

where $k = 2\pi/\lambda$. By controlling the progressive phase difference between the antenna elements by controlling ϕ_0 , the main beam of the linear antenna array can be steered in any desired direction. The detailed derivation of the array gain can be found in the preliminary work in [1]. Fig. 1 shows a plot of $|AF(\theta = \pi/2, \phi)|^2$ and $|AG(\theta = \pi/2, \phi)|$ for different values of ϕ_0 when $N_a = 2$. Note that the maximum value of $|AF(\theta = \pi/2, \phi)|^2$ is equal to $(N_a)^2$. It should also be noted that the maximum value of $|AG(\theta = \pi/2, \phi)|$ remains constant for different values of ϕ_0 , is equal to N_a times G_0 , and is independent of the element pattern.

4.3.2. SIR model with shadowing

The protocol model [28] has been widely used to model interference for channel assignment in wireless mesh networks [2–17]. This simplistic model assumes that interference is a binary phenomenon. The more accurate SINR (signal-to-interference-and-noise ratio) model considers the effect of cumulative interference [28]. The study in [34] recommends the use of the SINR model to obtain accurate performance results for multi-hop wireless networks. However neither of these interference models incorporates shadowing, which is needed to reflect the reality of signal propagation in wireless links. An improved physical model that accounts for shadowing is referred to as the *SINR model with shadowing*. SIR

(signal-to-interference ratio) can be used instead of SINR since co-channel interference is generally much stronger than noise. We use the *SIR model with shadowing* [18] to model interference in MRMC WMNs as realistically as possible. Note that in this model, the interference is controlled but it still exists. *Interference-free* communication in this model means that the desired incoming signal's SIR is above the required SIR threshold to be correctly received at the receiver.

The link transmission power or the received interference power is calculated using the *Free Space model with shadowing* for shorter distances and the *Two-Ray ground reflection model with shadowing* for longer distances, depending on the Euclidean distance between the nodes $d(x,y)$ in relation to the cross-over distance $Cross_over_dist$. If $d(x,y) \leq Cross_over_dist$, the Free Space model with shadowing is used, otherwise the Two-Ray model with shadowing is used. Using the Free Space model with shadowing, transmission power is

$$P_t = \frac{RxThresh(4\pi d)^2}{G_t G_r \lambda^2} \times 10^{-x/10}, \quad (3)$$

and received power is

$$P_r = \frac{P_t G_t G_r \lambda^2}{(4\pi d)^2}, \quad (4)$$

where x is a lognormal random variable. The transmission power using the Two-Ray model with shadowing is

$$P_t = \frac{RxThresh(d)^4}{G_t G_r h_t^2 h_r^2} \times 10^{-x/10}, \quad (5)$$

and received power is

$$P_r = \frac{P_t G_t G_r h_t^2 h_r^2}{(d)^4}, \quad (6)$$

where $RxThresh$ is the power threshold required by the radio interface of the receiver to correctly understand the received signal [35].

4.3.3. Conflict graph and matrix

An essential part of the method for channel assignment is the construction of the *conflict matrix* representing conflicts between the links involved in routing. The set of links involved in routing is L , so the conflict matrix is of size $|L| \times |L|$ and has elements that are either one (indicating a conflict between a pair of links; this appears as an edge in the conflict graph) or the maximum power received at a link from any other link. Our method for constructing the conflict graph and matrix for LAB-CA is given in [Algorithm 1](#). The nomenclature is: f (frequency); G_t (gain of transmitter); G_r (gain of receiver); h_t (transmitter antenna height); h_r (receiver antenna height); n (number of mesh nodes); $RxThresh_dBm$ (receiver threshold in dBm); $SIRThresh_dB$ (SIR threshold in dB); L (set of links involved in routing); $locations_x$ (set of x -coordinates of nodes); $locations_y$ (set of y -coordinates of nodes); σ (standard deviation for shadowing); OP (outage probability); N_a (number of antenna elements in the linear antenna array); and d_a (distance between the antenna elements of the array).

To determine the array gain AG_{ab} from node a to b using (1), we calculate the angle ϕ_{ab} between the nodes and use ϕ and ϕ_o equal to ϕ_{ab} . Due to reciprocity, AG_{ab} is the same as AG_{ba} . To check if link l_{pq} conflicts with link l_{xy} , we proceed as follows. We calculate $P_{r,xp}$ (power received at node x from node p), $P_{r,xq}$ (power received at node x from node q), $P_{r,yp}$ (power received at node y from node p), and $P_{r,yq}$ (power received at node y from node q) using (4) or (6). To calculate $P_{r,xp}$, we calculate $P_{t,pq}$ using (3) or (5), which is the transmission power required when node p is transmitting to q ; array gain AG_{px} from node p to x ; and array gain AG_{xp} from node x to

p . To calculate AG_{xp} using (1), we calculate ϕ_{xp} , the angle between node x and p ; ϕ_{xy} , the angle between node x and y ; and substitute them for ϕ and ϕ_o , respectively. If the ratio of the $RxThresh_mwatts$ (receiver threshold in mW) to the maximum of the four received powers at link l_{xy} from link l_{pq} is less than the required SIR threshold, a conflict is indicated between links l_{xy} and l_{pq} by placing a one in the conflict matrix. If this ratio is above the required SIR threshold, there could be no direct conflict between the two links and they could be active simultaneously over the same frequency channel. In this case, the maximum of the four received powers at link l_{xy} from link l_{pq} is placed in the conflict matrix for use later while building *weighted maximal independent sets* (WMAISs) during the minimum coloring stage.

As stated earlier, each radio interface of a multi-radio mesh node is equipped with an omni-directional antenna. For OAP-CA, a mesh node communicates with its neighbors using the circular radiation pattern of its unity-gain omni-directional antennas. So G_t and G_r are set equal to one for calculating P_t and P_r while constructing the conflict graph and matrix for OAP-CA.

4.4. Minimum coloring

Given the conflict graph $F(V_F, E_F)$, where vertices V_F represent wireless links between the mesh nodes and edges E_F represent the conflicts between wireless links, the minimum coloring stage of the channel assignment problem involves finding the minimum number of frequency channels to use such that there is no interference, i.e. no adjacent vertices are assigned the same frequency channel. This is identical to the standard minimum coloring problem, which is known to be NP-hard for general graphs [29].

The coloring problem is complicated by the fact that when there are multiple links using the same frequency channel, the cumulative interference may be enough to cause an unacceptable level of interference on some link using that channel, even though the interference on each pair of links is below the tolerance. We must account for the cumulative interference at every vertex in a WMAIS from all other vertices in this set. The *cumulative SIR* is the ratio of $RxThresh_mwatts$ to the sum of the maximum powers received at a vertex from all other vertices in the WMAIS, and must be greater than the required SIR threshold to avoid unacceptable interference. Note that the maximum received powers are available to us from the conflict matrix.

Our greedy heuristic for solving this extended coloring problem consists of these steps: (a) find a WMAIS of vertices in the conflict graph and assign the members of this set to the same frequency channel; (b) remove these vertices from the conflict graph; and (c) repeat until all vertices are assigned a frequency channel. The number of frequency channels required for interference-free communication among the mesh nodes is equal to the number of WMAISs. Since finding a maximum independent set is itself NP-hard [36], we also use heuristics for this step.

We use three randomized heuristic algorithms [18] that enforce the cumulative interference constraint at every vertex. They find WMAISs from the conflict graphs and matrices returned by OAP-CA and LAB-CA and use these to solve this extended coloring problem. The *Enhanced Maximum_Node_Degree_Start* algorithm selects a vertex from the conflict graph having the maximum number of conflicts with other vertices and introduces that vertex into the WMAIS under construction. If a vertex w does not conflict with vertices already in the WMAIS under construction, we add w and the vertices in the WMAIS to a temporary set. If the cumulative SIR at every vertex in the temporary set is greater than the required SIR threshold, we add w to the WMAIS. The *Enhanced Minimum_Node_Degree_Start* algorithm starts by selecting a vertex with the minimum number of conflicts, and the *Enhanced Random Start*

algorithm starts by selecting a vertex at random from the conflict graph. Ties for starting vertex are broken randomly.

Using these heuristics to find WMaSSs, the overall greedy minimum coloring heuristic is very quick, so we run each of the three algorithm variants multiple times on the conflict graph and take the best solution (i.e. requiring the fewest frequency channels) over all runs.

5. Beamforming-based channel assignment for heterogeneous mesh nodes

To model a more realistic WMN architecture, we extend our channel assignment framework in Section 4 to incorporate heterogeneous mesh nodes. We extend the *Select x for less than x TCA* [2], the multi-path routing formulation [11], and the method for constructing the conflict graph and matrix in Algorithm 1 to accommodate heterogeneous mesh nodes.

5.1. Extended select x for less than x TCA

We extend the *Select x for less than x TCA* to build the connectivity graph for LAB-CA_HT. Each mesh node broadcasts a *Hello* message at maximum transmission power containing its node ID and position over the control channel using the control radio. From the information in the received *Hello* messages, each mesh node arranges its neighboring nodes in ascending order of their distance, which results in its *maximum power neighbor table*. Each mesh node then sends its maximum power neighbor table along with its position, its node-degree x , and its node ID to the GW over the control channel using its control radio. Based on the node-degree x of a mesh node, the GW builds its *direct neighbor table* by selecting at least x nearest nodes as its communication neighbors. If required, the GW converts any uni-directional links in the direct neighbor tables of mesh nodes into bi-directional links, which results in their *final neighbor table*.

For a mesh node with a node-degree of 2 or 3, the GW ensures that it has at least 3 nearest nodes as its neighbors by using the *extended Select 3 for less than 3 TCA*; for a mesh node with a node-degree of 4, the GW ensures that it has at least 4 nearest nodes as its neighbors by using the *extended Select 4 for less than 4 TCA*; and so on. Since the *extended Select 2 for less than 2 TCA* mostly leads to a disconnected network, we use the *extended Select 3 for less than 3 TCA* for a mesh node with a node-degree of 2.

5.2. Extended multi-path routing formulation

To accommodate heterogeneous mesh nodes, all other constraints in the existing formulation of the multi-path routing problem remain the same except for the node-degree constraint. Let ND be the set of node-degrees of mesh nodes and nd_i be an input parameter denoting the node-degree of mesh node i . Then the following represent the constraints on the node-degrees of the mesh nodes in the WMN.

$$\sum_k z_{ki} + \sum_j z_{ij} \leq nd_i \quad \text{for all } i, \quad (7)$$

where $i, j, k \in V$, and $z_{ij} \in \{0,1\}$ is 1 when link between nodes i and j is used for routing and 0 otherwise.

5.3. Extended beamforming-based conflict graph and matrix

Algorithm 1 for constructing the conflict graph and matrix for LAB-CA is extended for LAB-CA_HT to accommodate heterogeneous mesh nodes. Added inputs in Algorithm 1 include ND , i.e. the set of node-degrees of mesh nodes. Note that while calculating the link transmission power in Step #10 of Algorithm 1, reciprocity cannot

be applied as AG_{ab} is no longer the same as AG_{ba} since the node-degrees of nodes a and b could be different. To calculate AG_{ab} , N_a is set equal to $ND(L(i,1))$, and to calculate AG_{ba} , N_a is set equal to $ND(L(i,2))$, where $L(i,1)$ represents the first node (or node a) in the i^{th} link in L ; $L(i,2)$ represents the second node (or node b) in the i^{th} link in L ; $ND(L(i,1))$ contains the node-degree of node a ; and $ND(L(i,2))$ contains the node-degree of node b .

The node-degrees of mesh nodes are also needed while calculating the received power. For example, to calculate the power received at node x from node p in Step #22 of Algorithm 1, the node-degree of node x is needed to know the number of antennas while calculating AG_{xp} and the node-degree of node p is needed to know the number of antennas while calculating AG_{px} since the node-degrees of nodes x and p could be different in a heterogeneous mesh network. N_a is set equal to $ND(L(i,1))$ while calculating AG_{xp} , and it is set equal to $ND(L(j,1))$ while calculating AG_{px} , where $L(i,1)$ represents the first node (or node x) in the i^{th} link in L , and $L(j,1)$ represents the first node (or node p) in the j^{th} link in L .

Fig. 2 is a plot of $|AG(\theta = \pi/2, \phi)|$ for different values of N_a when $\phi_o = 60^\circ$, showing that the beam formed by a six-antenna array is more focused than that formed by a three-antenna array.

6. Performance evaluation

The performance of LAB-CA is evaluated in comparison with OAP-CA for different *node-degree constraints* (NDCs) at different link data rates based on NCR in sparse mesh networks. For LAB-CA_HG vs. LAB-CA_HT, we compare performance in terms of *network throughput* (NT), the solution time of the routing stage, and NCR for different NDCs at different link data rates in sparse mesh networks.

The performance of LAB-CA_HT in sparse as well as dense mesh networks is evaluated in comparison with OAP-CA_HT in terms of NCR, *links-to-channels ratio* (LCR), network throughput, and solution time of the routing stage for different NDCs at a link data rate of 54 Mbps. We define *links-to-channels ratio* as the ratio of the number of links involved in routing and NCR. A higher LCR is better, e.g. an LCR of 3 indicates that 3 links use the same frequency channel on average. The worst-case LCR is 1, meaning that each link involved in routing requires a different frequency channel, so there is no spatial channel reuse. Note that OAP-CA_HT is the same as OAP-CA except for its connectivity graph and routing stages, which are described in Sections 5.1 and 5.2, respectively.

The impact of increasing the number of antennas in the linear antenna arrays of multi-radio mesh nodes on the performance of LAB-CA_HT is evaluated in terms of NCR in dense MRMCMMA WMNs for different N_a s (i.e. numbers of antennas) at a link data rate of 54 Mbps.

6.1. Experimental setup

6.1.1. Network topology

A *controlled random topology* (CRT) is used for the evaluation. A 500 m \times 500 m physical terrain is divided into cells and a mesh node is placed randomly within each cell using a uniform random distribution. For sparse mesh networks, twenty-five different CRTs consisting of 36-node networks are considered, and for dense mesh networks, twenty-five different CRTs consisting of 100-node networks are considered.

6.1.2. Software and hardware used

MATLAB version 7.8 [37] is used to implement the following algorithms: *Select x for less than x TCA*, conflict graph and matrix for OAP-CA, conflict graph and matrix for LAB-CA, heuristics

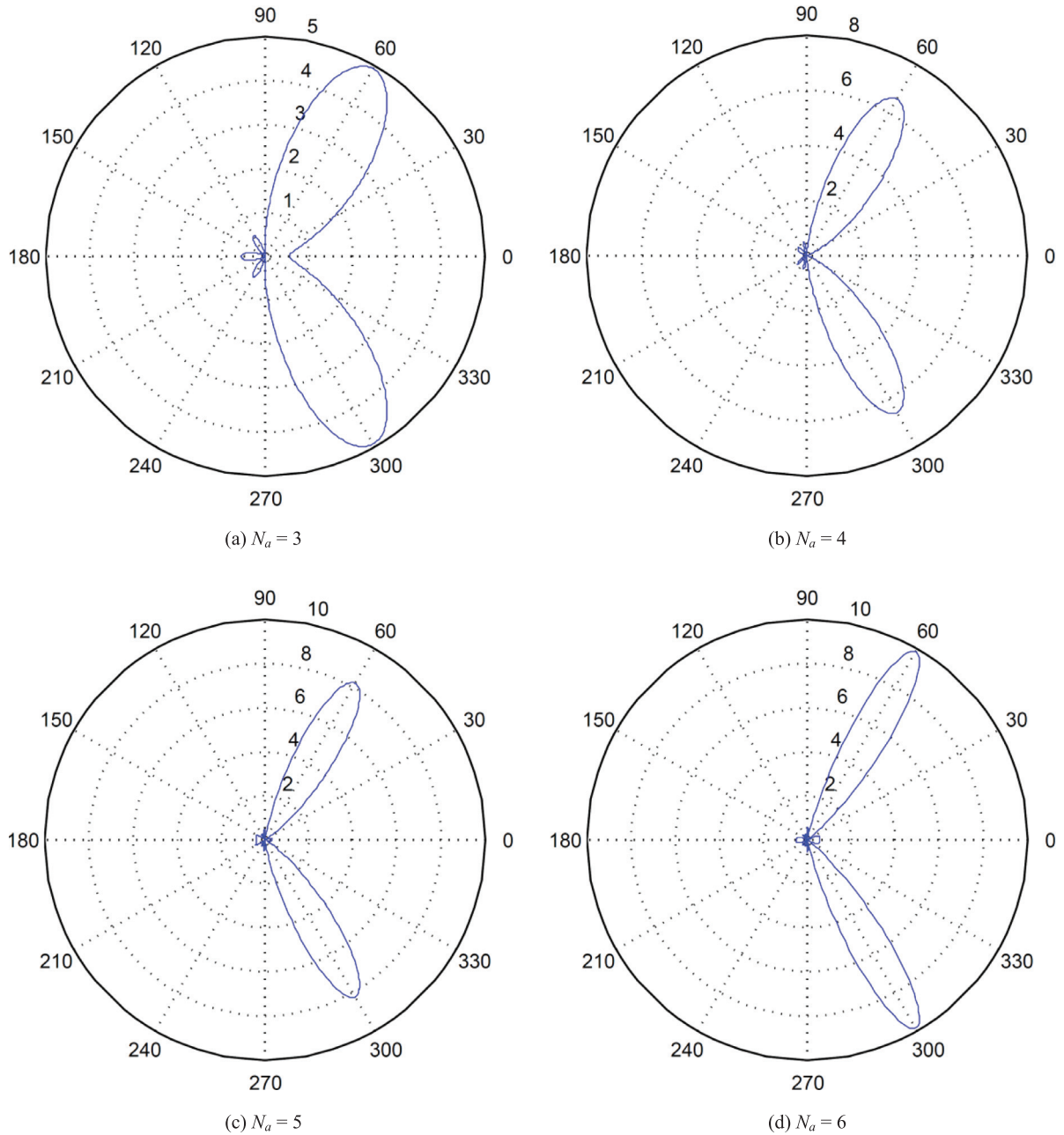


Fig. 2. Plot of $|AG(\theta=\pi/2, \phi)|$ for different values of N_a ($\phi_0=60^\circ$).

for extended minimum coloring with cumulative interference constraints, *extended Select x for less than x* TCA, and conflict graph and matrix for LAB-CA_HT.

The AMPL language [31] is used to express the mixed integer linear programming formulation of the multi-path routing problem and IBM’s CPLEX solver version 12.2 [32] is used to solve the resulting problem.

All software, including MATLAB, AMPL, and CPLEX, was run on a desktop PC having an Intel Core 2 Quad Q8200 processor running at 2.33 GHz, and 8 GB of memory. The operating system was Windows Vista Business with Service Pack 2.

6.1.3. Simulation parameters

For constructing the conflict graph, we assume the frequency to be 5.805 GHz; G_t and G_r to be 1 for OAP-CA; and h_t and h_r to

be 3 m. The receiver thresholds are taken as -79 , -74 , -70 , and -65 dBm for link data rates of 12, 24, 36, and 54 Mbps, respectively as per the IEEE 802.11a standard [38]. The SIR requirements are calculated as 5.78, 10.93, 13.20, and 18.42 dB for link data rates of 12, 24, 36, and 54 Mbps, respectively [18] [39]. σ is set to 3 dB, and OP is set to 10%. We use these reasonable assumptions to generate representative results, but our work can be applied to any scenario of multi-hop MRMC WMNs and is not limited to a specific standard.

We search for the first feasible solution of the network throughput for multi-path routing using the CPLEX solver. This significantly reduces the solution time of the routing stage at the cost of a small degradation in the network throughput.

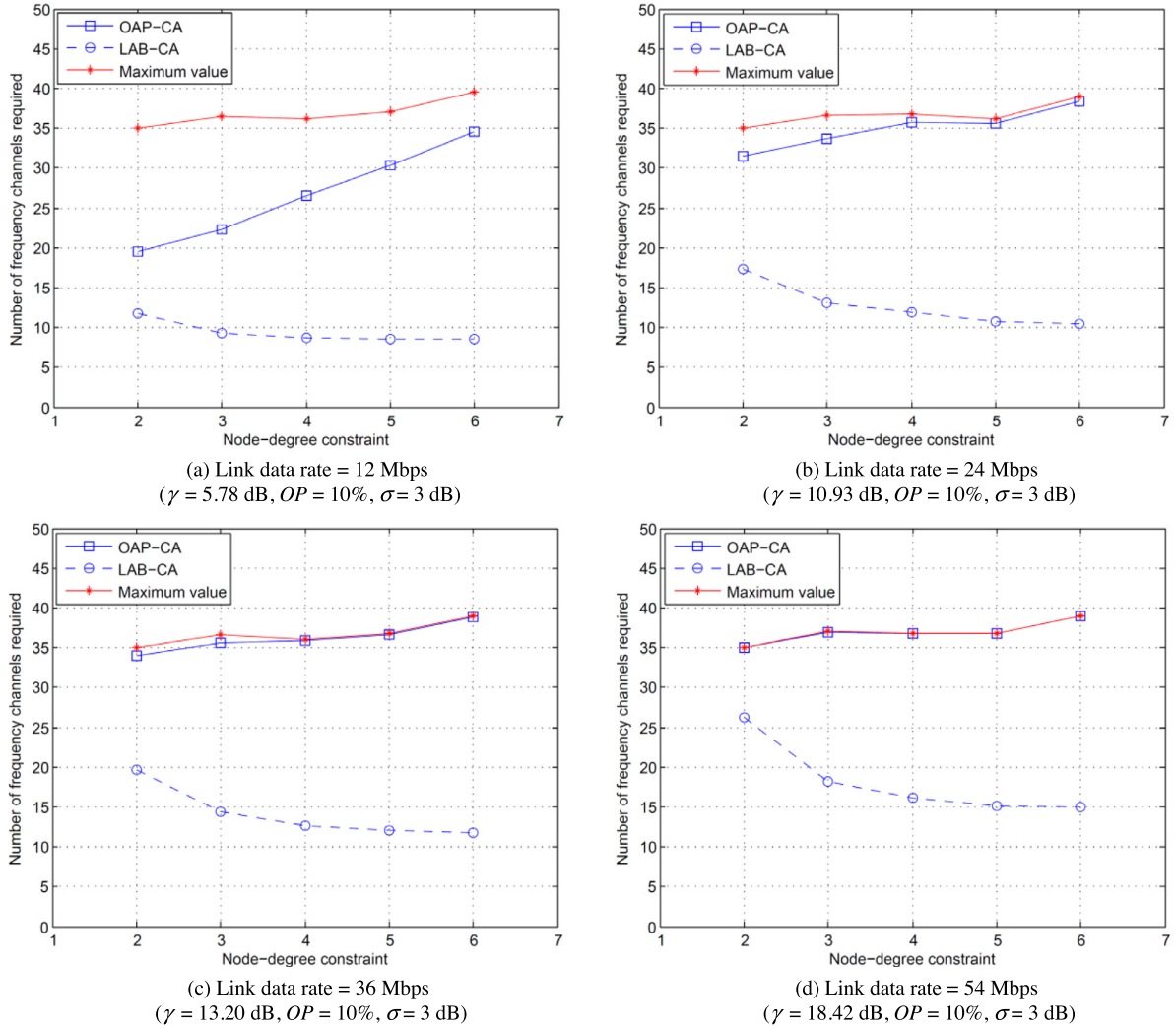


Fig. 3. NCR at different link data rates – OAP-CA vs. LAB-CA.

6.2. Results

6.2.1. OAP-CA vs. LAB-CA

We collected mean values and statistics on the 95% confidence intervals of the NCR for the 25 different CRTs used for both channel assignment methods. For brevity, mean values of NCR for different NDCs at different link data rates are graphed in Fig. 3 so that trends are immediately apparent. γ represents the SIR threshold, σ represents the standard deviation for shadowing, and OP represents the outage probability. The red line shows the worst case maximum value of NCR in which each link involved in routing requires a different frequency channel. As expected in theory, LAB-CA requires significantly fewer frequency channels than OAP-CA for all NDCs at all link data rates.

For a certain node-degree constraint, NCR for OAP-CA, as well as NCR for LAB-CA increases with γ as the link data rate increases. Higher γ means less tolerance for interference in the network. This results in more conflicts in the conflict graph, leading to a higher NCR. Also, NCR for OAP-CA increases with NDC. As NDC increases, more nodes which are farther away from a given node are selected as its data communication neighbors. This results in longer links in the connectivity graph. A longer link requires more transmission power, which causes more interference in the network. This results in more conflicts in the conflict graph, leading to a higher NCR. The

NCR for LAB-CA, on the other hand, decreases with NDC because the beam formed by the linear antenna array becomes narrower as the number of antennas increases with NDC. The higher the NDC, the larger the number of antennas and the narrower the beam formed by the array; hence there is better spatial reuse, fewer conflicts in the conflict graph, and lower NCR when using LAB-CA.

6.2.2. LAB-CA_HG vs. LAB-CA_HT

We collected mean values and 95% confidence intervals (CIs) of all measures for the 25 different CRTs used for both channel assignment methods. The solution times of the routing stage are presented in tabular form. For brevity, mean values of network throughput and NCR for different NDCs at different link data rates are graphed. The value “4, 2 to 4” for the NDC in a figure or a table means that all mesh nodes have a node-degree of four in LAB-CA_HG whereas in LAB-CA_HT, mesh nodes are randomly assigned a node-degree between two and four.

6.2.2.1. Solution time of the routing Stage. Table 1 compares the two channel assignment methods at different link data rates in terms of the solution time of the routing stage. LAB-CA_HT has slightly higher solution times than LAB-CA_HG. Note that a node-degree of two is a difficult constraint to satisfy during the routing of flows and due to the presence of such nodes in the heterogeneous

Table 1
Solution time of the routing stage – LAB-CA_HG vs. LAB-CA_HT.

Link Data Rate (Mbps)	NDC	Solution Time of the Routing Stage (secs)			
		LAB-CA_HG		LAB-CA_HT	
		Mean	95% CI	Mean	95% CI
12	3, 2 to 3	1.52	1.27–1.78	2.07	1.79–2.36
	4, 2 to 4	1.77	1.48–2.07	2.36	2.05–2.67
	5, 2 to 5	1.44	1.23–1.65	2.83	2.50–3.16
	6, 2 to 6	1.79	1.59–1.99	2.80	2.28–3.31
24	3, 2 to 3	1.57	1.33–1.81	2.10	1.83–2.37
	4, 2 to 4	1.77	1.45–2.09	2.29	2.04–2.54
	5, 2 to 5	1.91	1.40–2.42	2.94	2.52–3.36
	6, 2 to 6	1.92	1.68–2.16	2.63	2.07–3.18
36	3, 2 to 3	1.48	1.27–1.70	1.94	1.69–2.19
	4, 2 to 4	1.86	1.48–2.24	2.25	2.05–2.44
	5, 2 to 5	1.49	1.19–1.79	2.72	2.32–3.11
	6, 2 to 6	1.94	1.61–2.27	3.10	2.37–3.82
54	3, 2 to 3	1.61	1.39–1.83	2.09	1.84–2.33
	4, 2 to 4	2.19	1.76–2.63	2.55	2.28–2.82
	5, 2 to 5	1.85	1.43–2.28	3.16	2.67–3.65
	6, 2 to 6	2.49	2.00–2.97	3.53	2.90–4.15

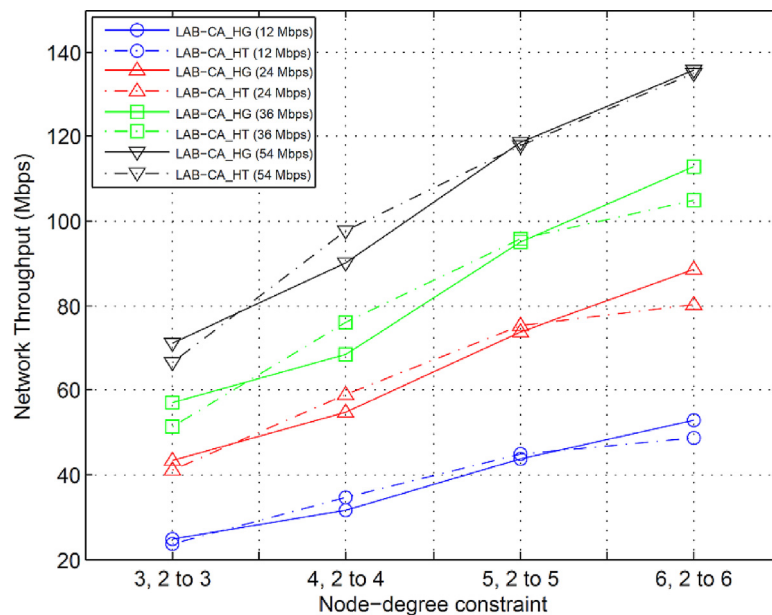


Fig. 4. Network Throughput (Mbps) at different data rates – LAB-CA_HG vs. LAB-CA_HT.

architecture, it takes the solver more time to find the solution for network throughput.

6.2.2.2. Network throughput. Fig. 4 compares the two channel assignment methods at different link data rates in terms of network throughput. These results show that the two methods have similar performance in terms of network throughput.

Table 2 compares the two channel assignment methods at different link data rates in terms of the number of controlled random topologies where the first feasible solution for network throughput is the optimum solution. Note that the channel assignment method that has more CRTs in which the first feasible solution is the optimum solution achieves a slightly better network throughput. For example, for NDC of “4, 2 to 4” at a link data rate of 54 Mbps, the number of CRTs in which the first feasible solution is the optimum solution is 13 for LAB-CA_HG and 16 for LAB-CA_HT in Table 2, and the corresponding network throughput is 90.17 Mbps for LAB-CA_HG and 97.79 Mbps for LAB-CA_HT.

6.2.2.3. Number of frequency channels required. Fig. 5 compares the two channel assignment methods at different link data rates in terms of NCR. LAB-CA_HT requires more frequency channels than LAB-CA_HG.

In LAB-CA_HG at a NDC of six, a mesh node uses all six antennas in its linear antenna array to form a beam. On the other hand, in LAB-CA_HT when the NDC is between two and six and a mesh node is randomly assigned a node-degree of two, it uses its two-antenna linear array to form a beam. More focused beams in LAB-CA_HG lead to better spatial reuse, fewer conflicts and lower NCR.

We also collected statistics on average link transmission power and $NCCM/|L|^2$ for the two channel assignment methods (Table 3), where NCCM is the number of conflicts in the conflict matrix and $|L|^2$ is the size of the conflict matrix. $NCCM/|L|^2$ indicates the fraction of possible conflicts. A lower $NCCM/|L|^2$ is better; its maximum value is 1 when the conflict graph is fully connected, meaning that all the elements in the conflict matrix are equal to 1.

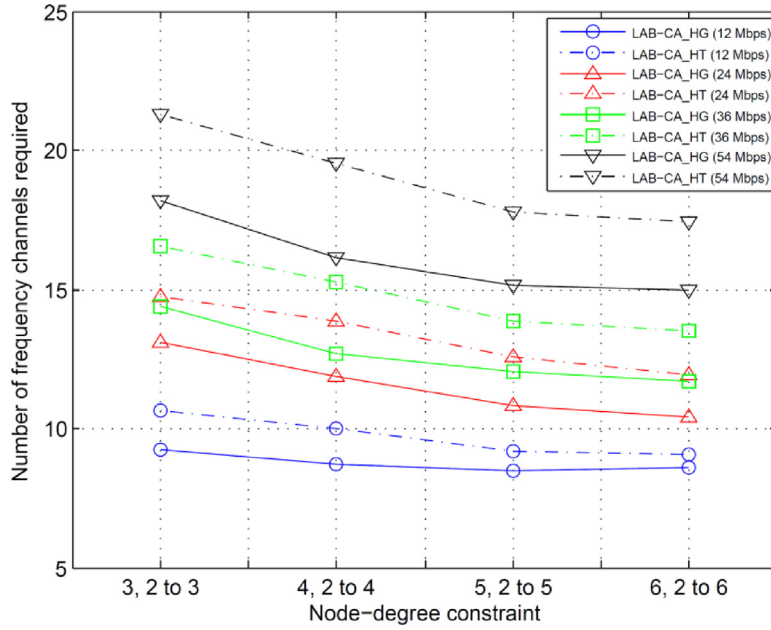


Fig. 5. NCR at different data rates – LAB-CA_HG vs. LAB-CA_HT.

Table 2

Number of CRTs with optimum solution of NT – LAB-CA_HG vs. LAB-CA_HT.

Link Data Rate (Mbps)	NDC	Number of CRTs with Optimum Solution of NT	
		LAB-CA_HG	LAB-CA_HT
12	3, 2 to 3	16	11
	4, 2 to 4	8	17
	5, 2 to 5	19	22
	6, 2 to 6	18	12
24	3, 2 to 3	17	10
	4, 2 to 4	11	15
	5, 2 to 5	19	20
36	6, 2 to 6	16	9
	3, 2 to 3	14	8
	4, 2 to 4	6	17
	5, 2 to 5	18	20
54	6, 2 to 6	17	12
	3, 2 to 3	19	8
	4, 2 to 4	13	16
	5, 2 to 5	21	19
	6, 2 to 6	16	13

The average link transmission power and $NCCM/|L|^2$ for both channel assignment methods decrease as NDC increases. The beam formed by the linear antenna array becomes narrower as the number of antennas increases with the increase in NDC, resulting in a decrease in $NCCM/|L|^2$. Also, the array gain of the linear antenna array increases as the number of antennas increases with the increase in NDC, which results in a decrease in the average link transmission power. The decrease in average link transmission power as well as $NCCM/|L|^2$ leads to a lower NCR.

$NCCM/|L|^2$ for LAB-CA_HG is lower than that for LAB-CA_HT due to the more focused beams in LAB-CA_HG, and results in a lower NCR for LAB-CA_HG. Also, for a given NDC, an increase in the receiver threshold (i.e. $RxThresh_{dBm}$) leads to an increase in the average link transmission power as the link data rate increases. A higher link transmission power causes more interference and more conflicts resulting in an increase in NCR for both channel assign-

ment approaches with the increase in link data rate for a given NDC.

6.2.3. OAP-CA_HT vs. LAB-CA_HT

We collected mean values and 95% confidence intervals of all measures for the 25 different CRTs for both channel assignment methods in sparse as well as dense scenarios; these are reported in tables. For this comparison, the link data rate is 54 Mbps.

6.2.3.1. Number of frequency channels required. Tables 4 and 5 compare NCR between LAB-CA_HT and OAP-CA_HT in sparse and dense mesh networks, respectively. PR_{NCR} in these tables represents the percentage reduction in NCR when using LAB-CA_HT and is given by

$$PR_{NCR} = \left(\frac{NCR_{OAP-CA_HT} - NCR_{LAB-CA_HT}}{NCR_{OAP-CA_HT}} \right) \times 100. \quad (8)$$

These results clearly show that LAB-CA_HT requires significantly fewer frequency channels as compared to OAP-CA_HT for all NDCs in sparse as well as dense mesh networks. In fact, it performs even better in dense mesh networks and provides a reduction of at least 58% in NCR.

Tables 6 and 7 compare the two channel assignment methods in terms of average link transmission power and $NCCM/|L|^2$ for sparse and dense scenarios, respectively. The average link transmission power and $NCCM/|L|^2$ for OAP-CA_HT increase with the increase in NDC. As NDC increases, more nodes which are farther away are selected as data communication neighbors of a given node. This results in longer links in the connectivity graph, which increases the average link transmission power for the network as well as $NCCM/|L|^2$, leading to a higher NCR. On the other hand, the average link transmission power and $NCCM/|L|^2$ for LAB-CA_HT decrease as NDC increases, thereby leading to a lower NCR.

6.2.3.2. Links-to-channels ratio. Table 8 compares LCR between sparse and dense mesh networks when using LAB-CA_HT. PI_{LCR} in this table represents the percentage improvement in LCR when using LAB-CA_HT in dense mesh networks and is given by

$$PI_{LCR} = \left(\frac{LCR_{dense} - LCR_{sparse}}{LCR_{sparse}} \right) \times 100. \quad (9)$$

Table 3
Average link transmission power and $NCCM/|L|^2$ – LAB-CA_HG vs. LAB-CA_HT.

Link Data Rate (Mbps)	NDC	LAB-CA_HG		LAB-CA_HT	
		Average Link Transmission Power (mW)	$NCCM/ L ^2$	Average Link Transmission Power (mW)	$NCCM/ L ^2$
12	3, 2 to 3	0.60	0.2356	0.87	0.2711
	4, 2 to 4	0.41	0.2345	0.67	0.2553
	5, 2 to 5	0.31	0.2297	0.54	0.2477
	6, 2 to 6	0.24	0.2300	0.47	0.2413
24	3, 2 to 3	1.87	0.4305	2.80	0.4980
	4, 2 to 4	1.32	0.3885	2.19	0.4593
	5, 2 to 5	0.98	0.3632	1.69	0.4160
	6, 2 to 6	0.76	0.3256	1.49	0.3882
36	3, 2 to 3	4.62	0.5190	7.01	0.6070
	4, 2 to 4	3.33	0.4605	5.30	0.5426
	5, 2 to 5	2.47	0.4274	4.24	0.4979
	6, 2 to 6	1.91	0.3896	3.69	0.4674
54	3, 2 to 3	14.62	0.7159	21.40	0.7974
	4, 2 to 4	10.52	0.6477	16.90	0.7266
	5, 2 to 5	7.69	0.6018	13.62	0.6918
	6, 2 to 6	6.07	0.5408	11.88	0.6545

Table 4
NCR in sparse mesh networks – OAP-CA_HT vs. LAB-CA_HT.

NDC	OAP-CA_HT		LAB-CA_HT		PR_{NCR}
	NCR	95% CI for NCR	NCR	95% CI for NCR	
2 to 3	36.00	35.66–36.34	21.28	20.59–21.97	40.9
2 to 4	37.56	37.12–38.00	19.52	18.88–20.16	48.0
2 to 5	36.40	35.83–36.97	17.80	17.28–18.32	51.1
2 to 6	38.20	37.30–39.10	17.44	16.83–18.05	54.3

Table 5
NCR in dense mesh networks – OAP-CA_HT vs. LAB-CA_HT.

NDC	OAP-CA_HT		LAB-CA_HT		PR_{NCR}
	NCR	95% CI for NCR	NCR	95% CI for NCR	
2 to 3	94.76	94.05–95.47	39.32	38.79–39.85	58.5
2 to 4	97.32	96.58–98.06	35.64	34.94–36.34	63.4
2 to 5	100.28	99.73–100.83	32.80	32.17–33.43	67.3
2 to 6	100.20	99.73–100.67	30.28	29.52–31.04	69.8

LAB-CA_HT has a higher LCR in dense mesh networks and provides an improvement of at least 49% in dense mesh networks as compared to sparse mesh networks.

As can be seen in Tables 6 and 7, the average link transmission powers for LAB-CA_HT in dense mesh networks are less than those in sparse mesh networks. Nodes in a dense mesh network are closely spaced. The links between the nodes in the connectivity graph are shorter, which leads to lower average link transmission powers, causing less interference, as reflected by a lower $NCCM/|L|^2$ in dense mesh networks as compared to sparse mesh networks. Less interference improves the spatial channel reuse

leading to a greater reduction in the number of frequency channels and a higher LCR in dense vs. sparse networks.

6.2.3.3. Network throughput. Tables 9 and 10 compare network throughput and *throughput per node* (TPN) respectively between sparse and dense mesh networks. Network throughput in dense mesh networks is similar to that in sparse mesh networks. Note that the total amount of flow in the network depends on the number of links for the GW node, which increases with an increase in NDC. This results in an increase in network throughput with an increase in NDC. At an NDC of 2 to 3, there are three links for the GW and the maximum network throughput is equal to *capacity per link* \times *number of links* = 24.73 Mbps \times 3 = 74.19 Mbps; at an NDC of 2 to 4, there are four links for the GW and the maximum network throughput is 98.92 Mbps; and so on. Note that there is a small degradation in the achieved network throughput as compared to its maximum value due to finding the first feasible solution as opposed to finding the optimum solution.

Table 10 shows that throughput per node in dense mesh networks is less than that in sparse mesh networks. Note that all mesh nodes, except the GW, are sources of flow and the GW is the sink of all flows. In Table 9, the maximum network throughput at an NDC of 2 to 3 is 74.19 Mbps. In a sparse mesh network, this maximum network throughput is shared by 35 sources, which results in a maximum throughput per node of 2.1197 Mbps. On the other hand, in a dense mesh network, this maximum network throughput is shared by 99 sources, which results in a lower maximum throughput per node of 0.7493 Mbps.

6.2.3.4. Solution time of the routing stage. The solution times of the routing stage for dense mesh networks are higher than those for sparse mesh networks, at about 169–350 seconds for dense mesh networks and 2.05–3.55 seconds for sparse mesh networks. The

Table 6
Average link transmission power and $NCCM/|L|^2$ in sparse mesh Networks – OAP-CA_HT vs. LAB-CA_HT.

NDC	L	OAP-CA_HT		LAB-CA_HT	
		Average Link Transmission Power (mW)	$NCCM/ L ^2$	Average Link Transmission Power (mW)	$NCCM/ L ^2$
2 to 3	36.04	351.10	0.9937	21.40	0.7974
2 to 4	37.60	398.68	0.9940	16.90	0.7266
2 to 5	36.44	445.89	0.9966	13.62	0.6918
2 to 6	38.24	476.66	0.9966	11.88	0.6545

Table 7
Average link transmission power and $NCCM/|L|^2$ in dense mesh networks – OAP-CA_HT vs. LAB-CA_HT.

NDC	L	OAP-CA_HT		LAB-CA_HT	
		Average Link Transmission Power (mW)	$NCCM/ L ^2$	Average Link Transmission Power (mW)	$NCCM/ L ^2$
2 to 3	99.96	115.80	0.9610	7.05	0.5910
2 to 4	101.72	129.71	0.9679	5.45	0.5219
2 to 5	103.16	146.58	0.9780	4.62	0.4846
2 to 6	102.56	162.49	0.9806	3.95	0.4437

Table 8
LCR using LAB-CA_HT – sparse vs. dense.

NDC	Sparse Mesh Networks		Dense Mesh Networks		Pl_{LCR}
	LCR	95% CI for LCR	LCR	95% CI for LCR	
2 to 3	1.70	1.65–1.76	2.54	2.51–2.58	49.4
2 to 4	1.94	1.87–2.01	2.86	2.80–2.92	47.4
2 to 5	2.06	2.00–2.12	3.15	3.09–3.21	52.9
2 to 6	2.21	2.13–2.28	3.40	3.32–3.48	53.8

Table 9
Network throughput (Mbps) – sparse vs. dense.

NDC	Sparse Mesh Networks		Dense Mesh Networks		Max. NT (Mbps)
	NT (Mbps)	95% CI for NT (Mbps)	NT (Mbps)	95% CI for NT (Mbps)	
2 to 3	66.40	62.90–69.90	62.49	57.56–67.41	74.19
2 to 4	97.79	97.14–98.45	93.30	88.56–98.05	98.92
2 to 5	118.06	113.63–122.50	118.91	115.11–122.71	123.65
2 to 6	135.08	128.04–142.12	147.42	145.87–148.98	148.38

number of links in the connectivity graph is much higher for dense mesh networks (e.g. 526 links in the connectivity graph of CRT #1 at an NDC of 2 to 6) than that for sparse mesh networks (e.g. 194 links in the connectivity graph of CRT #1 at an NDC of 2 to 6). This results in a much bigger routing problem for dense mesh networks, which causes the solver to take more time to find the solution for network throughput.

6.2.4. LAB-CA_HT in MPMC vs. MPMCMA WMNs

Table 11 shows the average link transmission power, $NCCM/|L|^2$, and NCR when using LAB-CA_HT in a MPMC vs. a MPMCMA dense WMN. For this comparison, link data rate is set at 54 Mbps. In the MPMC WMN architecture, a NDC of two for a mesh node indicates two data radio interfaces and two antennas for that node. In the MPMCMA WMN architecture, a NDC of two for a mesh node also indicates two data radios but the number of antennas in its antenna array is three or more. As in the MPMC WMN architecture, a mesh node in the MPMCMA WMN architecture having a NDC of two can communicate with at most two of its neighbors at the same time using its two data radios but using better (i.e. more focused) beams due to the three or more antennas in its linear antenna array.

Table 10
Throughput per node (Mbps) – sparse vs. dense.

NDC	Sparse Mesh Networks			Dense Mesh Networks		
	TPN (Mbps)	95% CI for TPN (Mbps)	Max. TPN (Mbps)	TPN (Mbps)	95% CI for TPN (Mbps)	Max. TPN (Mbps)
2 to 3	1.8972	1.7972–1.9972	2.1197	0.6312	0.5815–0.6809	0.7493
2 to 4	2.7941	2.7754–2.8128	2.8262	0.9424	0.8945–0.9904	0.9991
2 to 5	3.3732	3.2465–3.4999	3.5328	1.2011	1.1627–1.2395	1.2489
2 to 6	3.8595	3.6584–4.0605	4.2394	1.4891	1.4734–1.5048	1.4987

Note that N_a in Table 11 indicates the number of antennas in the linear antenna array of a multi-radio mesh node. N_a of “2 to 6” in a heterogeneous MPMC WMN architecture means that a mesh node is randomly assigned a node-degree between 2 and 6 and the number of antennas in its linear antenna array is equal to the number of its data radios. A mesh node that is randomly assigned a node-degree of six (or six antennas) in the heterogeneous MPMC WMN has seven antennas when N_a is “3 to 7” in the heterogeneous MPMCMA WMN in Table 11; eight antennas when N_a is “4 to 8”; and so on.

PR_{NCR} (i.e. the percentage reduction in NCR) in Table 11 is calculated using

$$PR_{NCR} = \left(\frac{NCR_{MPMC} - NCR_{MPMCMA}}{NCR_{MPMC}} \right) \times 100. \quad (10)$$

LAB-CA_HT performs better in MPMCMA vs. MPMC dense WMNs and a reduction of at least 20% in NCR is achieved when N_a is increased from “2 to 6” to “8 to 12”. As N_a increases, the array gain increases and the average link transmission power decreases. Also, the array beam becomes more focused with the increase in N_a , which reduces $NCCM/|L|^2$. The decrease in average link transmission power as well as $NCCM/|L|^2$ leads to a lower NCR in MPMCMA WMNs.

7. Conclusions

We develop a new and effective channel assignment method that improves the frequency channel utilization of MPMC WMNs at the expense of increased hardware complexity by incorporating beamforming directly into the conflict graph and matrix during interference modeling. LAB-CA significantly reduces the number of frequency channels required to ensure interference-free communication among the mesh nodes for achieving maximum network throughput. The experimental results show that LAB-CA significantly outperforms classical OAP-CA in terms of NCR.

We extend our channel assignment framework to incorporate heterogeneous mesh nodes in order to model a more realistic WMN architecture. The extended channel assignment method LAB-CA_HT significantly outperforms OAP-CA_HT in terms of NCR in sparse as well as dense mesh networks. Compared to sparse mesh networks, the throughput per node is lower and the solution times of the routing stage are higher in dense mesh networks. The throttling of the throughput per node in dense mesh networks can be alleviated by adding more gateways. Also, when using multiple gateways, mesh nodes in a dense mesh network can be divided

Table 11Average link transmission power, $NCCM/|L|^2$ and NCR when using LAB-CA_HT – MRMC vs. MRMCMA dense WMNs.

MRMC WMNs				MRMCMA WMNs				PR _{NCR}
N_a	Average Link Transmission Power (mW)	$NCCM/ L ^2$	NCR	N_a	Average Link Transmission Power (mW)	$NCCM/ L ^2$	NCR	
2 to 6	3.95	0.4437	30.28	3 to 7	2.38	0.3382	24.12	20.34
				4 to 8	1.61	0.2697	20.24	33.16
				5 to 9	1.17	0.2246	18.00	40.55
				6 to 10	0.90	0.1918	16.08	46.90
				7 to 11	0.71	0.1689	14.72	51.39
				8 to 12	0.57	0.1516	13.72	54.69

Algorithm 1 Conflict graph and matrix for LAB-CA.

```

Inputs:
•  $f, G_t, G_r, h_t, h_r, n, RxThresh\_dBm, SIRThresh\_dB, L, locations\_x, locations\_y, \sigma, OP, N_a, d_a.$ 
Output:
•  $conflict\_matrix$ : Conflict graph
BEGIN
1.  $RxThresh\_mwatts \leftarrow 10^{(RxThresh\_dBm/10)}, m \leftarrow |L|, SIRThresh \leftarrow 10^{(SIRThresh\_dB/10)}$ 
2. For  $i = 1$  to  $n$ :
3.   For  $j = 1$  to  $n$ :
4.      $dist\_all(i,j) \leftarrow$  distance between node  $i$  and node  $j$ 
5.   end For
6. end For
7. For  $i = 1$  to  $m$ :
8.    $L(i,3) \leftarrow$  distance between the nodes of link  $i$ 
9.    $L(i,4) \leftarrow AG_{ab} \leftarrow$  array gain of  $beam_{ab}$  for nodes  $a$  and  $b$  of link  $i$  using (1)
10.   $L(i,5) \leftarrow P_{t,ab}$  for link  $i$  with  $G_t$  and  $G_r$  equal to  $AG_{ab}$  using (3) or (5)
11. end For
12. Initialize an  $m \times m$   $conflict\_matrix$  of all ones
13. For  $i1 = 1$  to  $m$ :
14.   Initialize an empty conflict table
15.   For  $j = 1$  to  $m$ :
16.      $conflict\_table(j,1) \leftarrow$  node  $x$  of link  $i1$ 
17.      $conflict\_table(j,2) \leftarrow$  node  $y$  of link  $i1$ 
18.      $conflict\_table(j,3) \leftarrow$  node  $p$  of link  $j$ 
19.      $conflict\_table(j,4) \leftarrow$  node  $q$  of link  $j$ 
20.      $AG_{xp} \leftarrow$  array gain of  $beam_{xy}$  with  $\phi = \phi_{xp}$  and  $\phi_o = \phi_{xy}$  using (1)
21.      $AG_{px} \leftarrow$  array gain of  $beam_{pq}$  with  $\phi = \phi_{px}$  and  $\phi_o = \phi_{pq}$  using (1)
22.      $P_{r,xp} \leftarrow$  power received at  $x$  from  $p$  with  $G_t = AG_{px}, G_r = AG_{xp}$  and  $P_{t,pq} = L(j,5)$  using (4) or (6)
23.      $conflict\_table(j,5) \leftarrow P_{r,xp}$ 
24.      $AG_{xq} \leftarrow$  array gain of  $beam_{xy}$  with  $\phi = \phi_{xq}$  and  $\phi_o = \phi_{xy}$  using (1)
25.      $AG_{qx} \leftarrow$  array gain of  $beam_{qp}$  with  $\phi = \phi_{qx}$  and  $\phi_o = \phi_{qp}$  using (1)
26.      $P_{r,xq} \leftarrow$  power received at  $x$  from  $q$  with  $G_t = AG_{qx}, G_r = AG_{xq}$  and  $P_{t,qp} = L(j,5)$  using (4) or (6)
27.      $conflict\_table(j,6) \leftarrow P_{r,xq}$ 
28.      $AG_{yp} \leftarrow$  array gain of  $beam_{yx}$  with  $\phi = \phi_{yp}$  and  $\phi_o = \phi_{yx}$  using (1)
29.      $AG_{py} \leftarrow$  array gain of  $beam_{pq}$  with  $\phi = \phi_{py}$  and  $\phi_o = \phi_{pq}$  using (1)
30.      $P_{r,yp} \leftarrow$  power received at  $y$  from  $p$  with  $G_t = AG_{py}, G_r = AG_{yp}$  and  $P_{t,pq} = L(j,5)$  using (4) or (6)
31.      $conflict\_table(j,7) \leftarrow P_{r,yp}$ 
32.      $AG_{yq} \leftarrow$  array gain of  $beam_{yx}$  with  $\phi = \phi_{yq}$  and  $\phi_o = \phi_{yx}$  using (1)
33.      $AG_{qy} \leftarrow$  array gain of  $beam_{qp}$  with  $\phi = \phi_{qy}$  and  $\phi_o = \phi_{qp}$  using (1)
34.      $P_{r,yq} \leftarrow$  power received at  $y$  from  $q$  with  $G_t = AG_{qy}, G_r = AG_{yq}$  and  $P_{t,qp} = L(j,5)$  using (4) or (6)
35.      $conflict\_table(j,8) \leftarrow P_{r,yq}$ 
36.      $conflict\_table(j,9) \leftarrow \max(P_{r,xp}, P_{r,xq}, P_{r,yp}, P_{r,yq})$ 
37.      $conflict\_table(j,10) \leftarrow RxThresh\_mwatts / \max(P_{r,xp}, P_{r,xq}, P_{r,yp}, P_{r,yq})$ 
38.   end For
39.   For  $i2 = 1$  to  $m$ :
40.     If  $conflict\_table(i2,10) > SIRThresh$ :
41.        $conflict\_matrix(i1,i2) \leftarrow conflict\_table(i2,9)$ 
42.     end If
43.   end For
44. end For
45. Output  $conflict\_matrix$ 
END

```

into groups, one group per gateway. This will divide the computational effort among the multiple gateways, which will reduce the solution times. As part of our future work, we plan to incorporate multiple gateways in our channel assignment framework.

We study the impact of increasing the number of antennas in the linear antenna arrays of the multi-radio mesh nodes on the

performance of LAB-CA_HT in terms of NCR in dense MRMCMA WMNs. The results show that a significant reduction in the number of frequency channels is achieved in MRMCMA vs. MRMC dense mesh networks when the number of antennas in the linear antenna arrays of mesh nodes is increased. By increasing the number

of antenna elements in the array, the space dimension can be effectively used to reduce the number of frequency channels.

References

- [1] A.U. Chaudhry, R.H.M. Hafez, J.W. Chinneck, Significantly reducing the number of frequency channels required for wireless mesh networks using beamforming, *IEEE WCNC*, 2014.
- [2] A.U. Chaudhry, N. Ahmad, R.H.M. Hafez, Improving throughput and fairness by improved channel assignment using topology control based on power control for multi-radio multi-channel wireless mesh networks, *EURASIP J. Wireless Commun. Netw.* 155 (2012).
- [3] A.U. Chaudhry, R.H.M. Hafez, O. Aboul-Magd, S.A. Mahmoud, Throughput improvement in multi-radio multi-channel 802.11a-based wireless mesh networks, *IEEE Globecom*, 2010.
- [4] A. Raniwala, K. Gopalan, T. Chiueh, Centralized channel assignment and routing algorithms for multi-channel wireless mesh networks, *ACM SIGMOBILE MC2R* 8 (2) (2004) 50–65.
- [5] P. Kyasanur, N. Vaidya, Routing and interface assignment in multi-channel multi-interface wireless networks, *IEEE WCNC*, 2005.
- [6] A. Raniwala, T. Chiueh, Architecture and algorithms for an IEEE 802.11-based multi-channel wireless mesh network, *IEEE INFOCOM*, 2005.
- [7] K. Ramachandran, E. Belding, K. Almeroth, M. Buddhikot, Interference-aware channel assignment in multi-radio wireless mesh networks, *IEEE INFOCOM*, 2006.
- [8] H. Skalli, S. Ghosh, S.K. Das, L. Lenzini, M. Conti, Channel assignment strategies for multi-radio wireless mesh networks: issues and solutions, *IEEE Commun. Mag.* 45 (11) (2007) 86–95.
- [9] S. Avallone, I.F. Akyildiz, A channel assignment algorithm for multi-radio wireless mesh networks, *Comput. Commun.* 31 (7) (2008) 1343–1353.
- [10] A.P. Subramanian, H. Gupta, S.R. Das, C. Jing, Minimum interference channel assignment in multiradio wireless mesh networks, *IEEE Trans. Mobile Comput.* 7 (12) (2008) 1459–1473.
- [11] A.U. Chaudhry, J.W. Chinneck, R.H.M. Hafez, On the number of channels required for interference-free wireless mesh networks, *EURASIP J. Wireless Commun. Netw.* 229 (2013).
- [12] M.K. Marina, S.R. Das, A.P. Subramanian, A topology control approach for utilizing multiple channels in multi-radio wireless mesh networks, *Comput. Netw.* 54 (2) (2010) 241–256.
- [13] A. Giannoulis, T. Salonidis, E. Knightly, Congestion control and channel assignment in multi-radio wireless mesh networks, *IEEE SECON*, 2008.
- [14] A.H.M. Rad, V.W.S. Wong, Cross-layer fair bandwidth sharing for multi-channel wireless mesh networks, *IEEE Trans. Wireless Commun.* 7 (9) (2008) 3436–3445.
- [15] X.Y. Li, A. Nusairat, Y. Wu, Y. Qi, J.Z. Zhao, X. Chu, Y. Liu, Joint throughput optimization for wireless mesh networks, *IEEE Trans. Mobile Comput.* 8 (7) (2009) 895–909.
- [16] W. Wu, J. Luo, M. Yang, L.T. Yang, Joint interface placement and channel assignment in multi-channel wireless mesh networks, *IEEE ISPA*, 2012.
- [17] J. Chen, J. Jia, Y. Wen, D. Zhao, J. Liu, A genetic approach to channel assignment for multi-radio multi-channel wireless mesh networks, *ACM/SIGEVO GEC*, 2009.
- [18] A.U. Chaudhry, R.H.M. Hafez, J.W. Chinneck, On the impact of interference models on channel assignment in multi-radio multi-channel wireless mesh networks, *Ad Hoc Netw.* 27 (2015) 68–80.
- [19] S.M. Das, H. Pucha, D. Koutsonikolas, Y.C. Hu, D. Peroulis, DMesh: Incorporating practical directional antennas in multi-channel wireless mesh networks, *IEEE J. Sel. Areas Commun.* 24 (11) (2006) 2028–2039.
- [20] Z. Zhang, Pure directional transmission and reception algorithms in wireless ad hoc networks with directional antennas, *IEEE ICC*, 2005.
- [21] A. Capone, I. Filippini, F. Martignon, Joint routing and scheduling optimization in wireless mesh networks with directional antennas, *IEEE ICC*, 2008.
- [22] Q. Dong, Y. Bejerano, Building robust nomadic wireless mesh networks using directional antennas, *IEEE INFOCOM*, 2008.
- [23] Q. Liu, X. Jia, Y. Zhou, Topology control for multi-channel multi-radio wireless mesh networks using directional antennas, *Wireless Netw.* 17 (1) (2011) 41–51.
- [24] B. Hamdaoui, K.G. Shin, Throughput behavior in multihop multiantenna wireless networks, *IEEE Trans. Mobile Comput.* 8 (11) (2009) 1480–1494.
- [25] M. Yazdanpanah, C. Assi, Y. Shayan, Cross-layer optimization for wireless mesh networks with smart antennas, *Comput. Commun.* 34 (16) (2011) 1894–1911.
- [26] Q. Kuang, J. Speidel, H. Droste, Joint base-station association, channel assignment, beamforming and power control in heterogeneous networks, *IEEE VTC*, 2012.
- [27] E. Zeydan, D. Kivanc-Tureli, U. Tureli, Joint iterative channel allocation and beamforming algorithm for interference avoidance in multiple-antenna ad hoc networks, *IEEE MILCOM*, 2007.
- [28] P. Gupta, P.R. Kumar, The capacity of wireless networks, *IEEE Trans. Inf. Theory* 46 (2) (2000) 388–404.
- [29] R.M. Karp, Reducibility among combinatorial problems, in: *Complexity of Computer Computations*, Plenum Press, New York, 1972, pp. 85–103.
- [30] Y. Xiao, J. Rosdahl, Throughput and delay limits of IEEE 802.11, *IEEE Commun. Lett.* 6 (8) (2002) 355–357.
- [31] R. Fourer, D. Gay, B. Kernighan, *AMPL: A Modeling Language for Mathematical Programming*, Brooks/Cole, Belmont, CA, 2003.
- [32] IBM ILOG CPLEX. [Online]. Available: <http://www-01.ibm.com/software/commerce/optimization/cplex-optimizer/index.html>
- [33] C.A. Balanis, *Antenna Theory, Analysis and Design*, 3rd edn., Wiley-Interscience, Hoboken, NJ, 2005.
- [34] A. Iyer, C. Rosenberg, A. Karnik, What is the right model for wireless channel interference? *IEEE Trans. Wireless Commun.* 8 (5) (2009) 2662–2671.
- [35] T. Rappaport, *Wireless Communications: Principles and Practice*, 2nd edn., Prentice Hall, Upper Saddle River, NJ, 2002.
- [36] M.R. Garey, D.S. Johnson, L. Stockmeyer, Some simplified NP-complete graph problems, *Theor. Comput. Sci.* 1 (3) (1976) 237–267.
- [37] The MathWorks Inc., *MATLAB® Reference Guide*, Natick, MA, 1992.
- [38] Part 11: Wireless LAN MAC and PHY Specifications, *IEEE Std 802.11* (2007) (Revision of IEEE Std 802.11 (1999)).
- [39] R.V. Nee, R. Prasad, *OFDM for Wireless Multimedia Communications*, Artech House Publishers, 2000.



Aizaz U. Chaudhry completed his PhD in Electrical and Computer Engineering from Carleton University, Ottawa, Canada, in July 2015. He received his MSc degree in Electrical and Computer Engineering from Carleton University in August 2010, and his BSc degree in Electrical Engineering from University of Engineering and Technology, Lahore, Pakistan, in November 1998. He has several years of professional experience in Philips, Siemens, and other telecommunications companies. He conducts research in the area of wireless mesh networks with a focus on topology control, routing, interference modeling, channel assignment, and optimization of multi-radio multi-channel multi-antenna wireless mesh networks.



Roshdy H.M. Hafez obtained the PhD in Electrical Engineering from Carleton University, Ottawa, Canada. He joined the Department of Systems and Computer Engineering at Carleton University as an assistant professor, and is now a full professor. Professor Hafez has many years of experience in the areas of wireless communications, RF and spectrum engineering. His current research focuses on broadband wireless networking, 3G/4G, wireless mesh and sensor networks. He acts as a consultant to Industry Canada, CRC, and other telecommunications companies. Between 1994 and 2000, he was actively involved and led projects in federal/provincial centers of excellence: TRIO, CITR and CITO.



John W. Chinneck is a professor in the Department of Systems and Computer Engineering. His degrees are from the University of Waterloo in Systems Design Engineering (BASC 1977, MASC 1978, PhD 1983). Professor Chinneck conducts research in the general area of applied optimization, including various applications in engineering. He is a member of the advisory board and former Editor-in-Chief (2007-2012) of the INFORMS Journal on Computing, a member of the editorial board for the journal Constraints, and a past member of the editorial board for Computational Management Science. He is a past Chair (2005-2007) of the INFORMS Computing Society.